

Rupture Reactivation during the 2011 M_w 9.0 Tohoku Earthquake: Dynamic Rupture and Ground-Motion Simulations

by Percy Galvez,* Luis A. Dalguer, Jean-Paul Ampuero, and Domenico Giardini

Abstract Near-source ground-motion observations and kinematic source inversions suggest that the rupture process of the 2011 M_w 9.0 Tohoku earthquake involved rupture reactivation, that is, repeated rupture nucleation in the same hypocentral area. This unusual phenomenon may have provided a second breath to the rupture that enhanced its final size. Here, we propose that rupture reactivation may have been governed by a slip-weakening friction model with two sequential strength drops, the second one being activated at large slip. Such frictional behavior has been previously observed in laboratory experiments and attributed to pressurization of fault-zone fluids by mineral decomposition reactions activated by shear heating, such as dehydration and decarbonation. Further evidence of this double-slip-weakening friction model is obtained here from the dynamic stress changes in the hypocentral region derived from a finite source inversion model. We incorporate this friction model in a dynamic rupture simulation comprising two main asperities constrained by source inversion models and several deep small asperities constrained by backprojection source imaging studies. Our simulation produces ground-motion patterns along the Japanese coast consistent with observations and rupture patterns consistent with a kinematic source model featuring rupture reactivation. The deep small asperities serve as a bridge to connect the two main asperities, and the rupture reactivation mechanism is needed to reproduce the observed ground-motion pattern. Therefore, we argue that rupture reactivation during the 2011 Tohoku earthquake is consistent with a second strength drop, possibly caused by activation of thermochemical weakening processes at large slip.

Online Material: Movie of simulated rupture and wave propagation and ground velocities recorded at the KiK-net and K-NET seismic networks.

Introduction

The 11 March 2011 M_w 9 Tohoku earthquake occurred in the subduction zone between the Pacific and North American plates in northeastern Honshu, Japan. This giant event was recorded by a vast Global Positioning System (GPS) and seismic network, providing a unique opportunity to study the complex rupture process of a megathrust event (e.g., Ide *et al.*, 2011; Simons *et al.*, 2011; Tajima *et al.*, 2013). Visual inspection of the strong ground motion recorded by the K-NET and KiK-net networks and the high-rate 1 Hz GPS displacements recorded by the GNSS Earth Observation Network System (GEONET) network along the Japanese coast clearly show two groups of waves (S1 and S2 in Fig. 1) arriving about 40 s apart in both the Miyagi and Iwate regions.

A third group of waves (S3 in Fig. 1) is observed further south in the Ibaraki and Chiba regions. These observations, together with kinematic source inversion models and backprojection source imaging results (e.g., Ide *et al.*, 2011; Ishii, 2011; Koketsu *et al.*, 2011; Lee *et al.*, 2011; Meng *et al.*, 2011; Simons *et al.*, 2011; Suzuki *et al.*, 2011; Roten *et al.*, 2012; Yagi *et al.*, 2012), indicate that the Tohoku earthquake featured complex rupture patterns involving multiple rupture fronts. These studies collectively reveal three remarkable features: (1) large shallow slip exceeding 40 m near the trench; (2) depth-dependent frequency content of seismic radiation with stronger high-frequency radiation in the deeper region and larger low-frequency slip at shallow depth; and (3) repeated slip in the region near and up-dip of the hypocenter.

Within the framework of dynamic rupture models, a number of studies have proposed possible mechanisms to explain these unusual rupture features. Although shallow mega-

*Now at the AECOM, Seismology Department, Ringstrasse 2, 4600, Olten Switzerland.

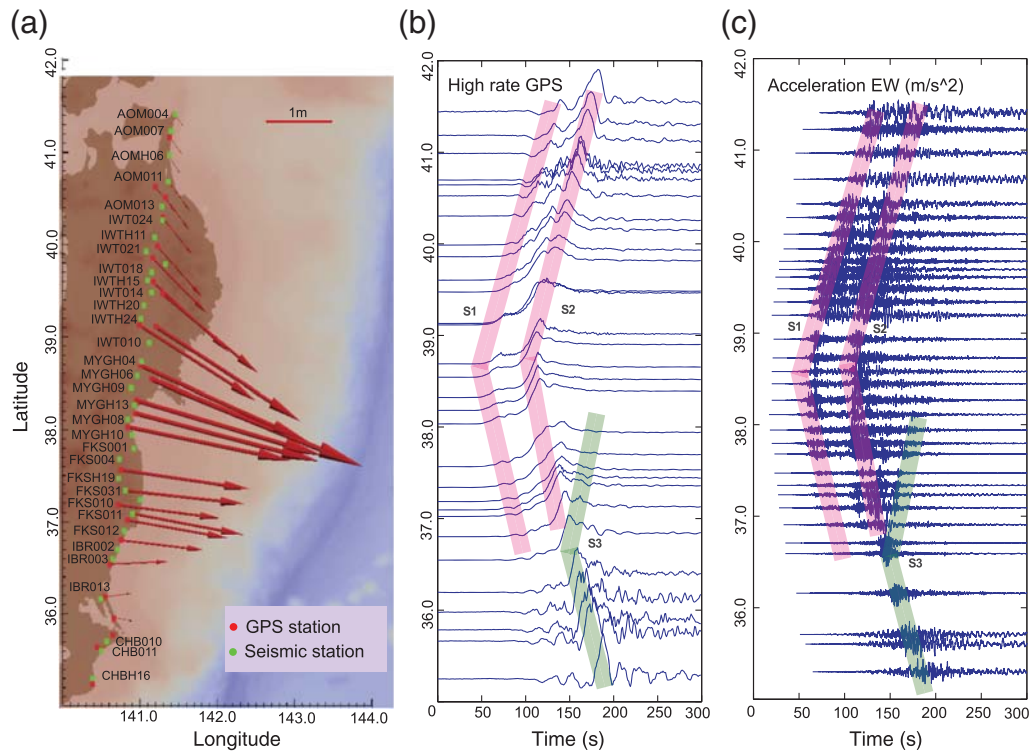


Figure 1. Ground-motion patterns of the 2011 Tohoku earthquake revealed by regional data. (a) Location of selected KiK-net and K-NET seismic stations (green squares) and GPS Earth Observation Network System (GEONET) Global Positioning System (GPS) stations (red squares) along the coast of Tohoku, Japan, and coseismic horizontal displacements (red arrows). (b) East–west displacement time series from 1 Hz GPS records. (c) East–west ground acceleration time series recorded by KiK-net and K-NET networks, low-pass filtered below 3 Hz. The pink bands in (b) and (c) indicate the first (S1) and second (S2) groups of seismic waves observed in the records. The green bands (S3) indicate the third group of waves observed onshore of the southern part of the rupture.

thrusts generally display velocity-strengthening friction due to the presence of sediments in the fault zone (e.g., Marone and Scholz, 1988; Oleskevich *et al.*, 1999), which promotes stable sliding, it is now recognized that sufficiently energetic dynamic ruptures can break through frictionally stable regions and low-stress regions (Kaneko *et al.*, 2010). The possibility of large slip near the trench can be further enhanced by dynamic stresses in the subduction wedge associated with sea-floor effects (Kozdon and Dunham, 2013; Huang *et al.*, 2014) and by dynamic weakening mechanisms operating at large slip or slip velocity in materials that are velocity strengthening at low speed (Mitsui, Kato, *et al.*, 2012; Noda and Lapusta, 2013; Cubas *et al.*, 2015). Enhanced high-frequency radiation at depth has been attributed to the presence of deep asperities on the megathrust (Mitsui, Iio, and Fukahata, 2012; Huang *et al.*, 2013, 2014) and its deprivation at shallow depth to thermal pressurization (e.g., Noda and Lapusta, 2013) and inelastic failure in the wedge (Ma and Hirakawa, 2013).

Repeated slip during the Tohoku earthquake has been mostly characterized as a rupture front backpropagating down-dip after the initial up-dip front reached the trench (Ide *et al.*, 2011). This phenomenon is usually found in dynamic rupture simulations of dipping faults and is caused by free surface effects (e.g., Dalguer *et al.*, 2001a,b; Huang *et al.*, 2014). Some observational studies conclude instead

that repeated slip occurred by repeated nucleation of rupture near the initial hypocenter. The presence of two sequential rupture fronts starting from the same hypocentral area during the Tohoku earthquake, a phenomenon denoted here as “rupture reactivation,” was first reported by Lee *et al.* (2011) in a kinematic source inversion study based on teleseismic, strong ground motion, and GPS data. The feature is illustrated in Figure 2a (see also Gabriel *et al.*, 2012), which shows the spatiotemporal evolution of slip velocity along a cross section of the fault oriented along-dip and passing through the hypocenter. Two rupture fronts emerge from the hypocenter area (black lines): the first one propagates mainly toward the trench, and the second one starts 40–50 s after the earthquake origin time and propagates bilaterally. Lee *et al.* (2011) parametrized the slip velocity functions in their source inversion by multiple time windows. Rupture reactivation is also apparent in another source inversion model derived from teleseismic, strong motion, and geodetic data (Koketsu *et al.*, 2011), in backprojection source imaging results based on data from the Metropolitan Seismic Observation Network (MeSO-net) in the Tokyo metropolitan area (Honda *et al.*, 2011), and in a source model inferred from regional ground-motion data by an iterative deconvolution and stacking technique (Zhang *et al.*, 2014). A common methodological aspect of these studies is their allowance for

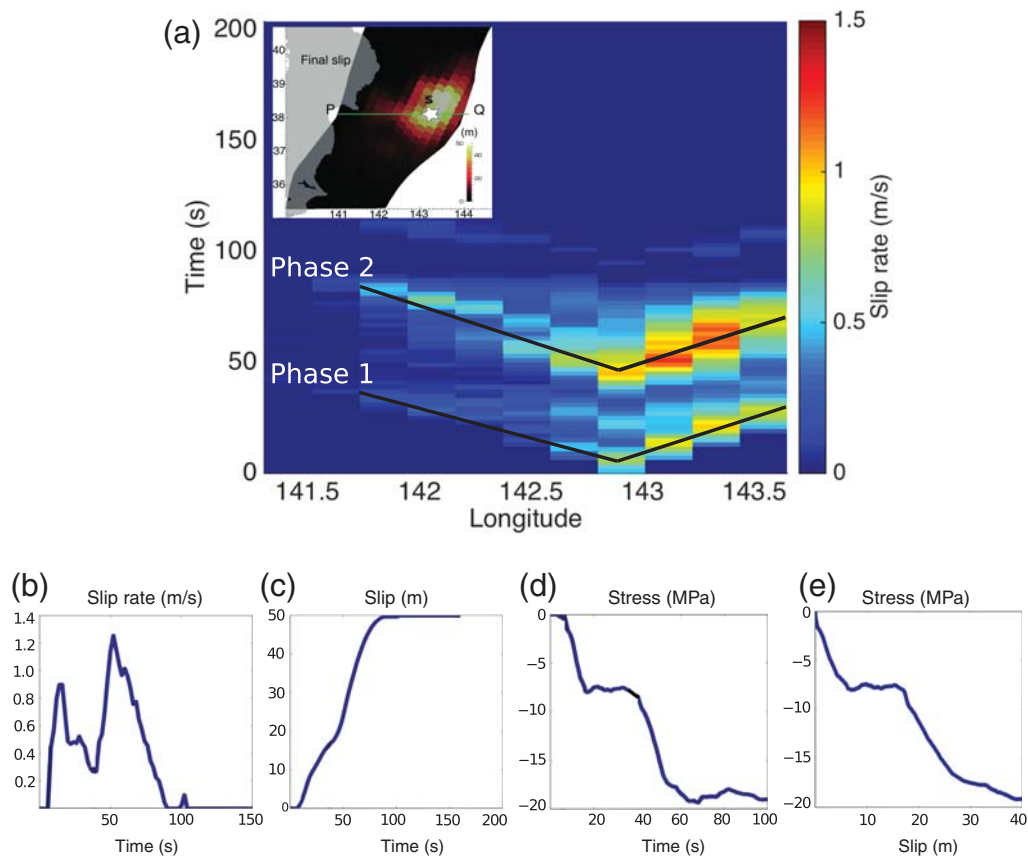


Figure 2. (a) Spatiotemporal evolution of slip velocity along the longitudinal cross section passing through the hypocenter (section PQ in the inset map), derived directly from the kinematic source model of [Lee et al. \(2011\)](#). Two rupture fronts emerge at the hypocenter area (phases 1 and 2, indicated by black lines), defining a rupture reactivation phenomenon. The inset also shows the final slip from this kinematic model and the epicenter location (white star). (b–e) Time histories of slip rate, slip and computed stress change, and stress change versus slip curve around the hypocenter.

multiple rupture fronts by either an unrestricted parameterization or a nonparametric description of the source.

Two mechanical models have been proposed to explain rupture reactivation: rupture in a heterogeneous initial stress field ([Goto et al., 2012](#)) and renucleation by a growing stress concentration left behind an initial self-similar slip pulse ([Gabriel et al., 2012](#)). Here, we develop a new rupture reactivation model based on a double-slip-weakening friction law similar to that introduced by [Kanamori and Heaton \(2000\)](#). These authors proposed that melting or fluid pressurization induced by frictional heating can reduce fault strength when slip exceeds a certain critical slip distance (D_r). They argued that, when superimposed to the conventional (isothermal) slip-weakening process with shorter critical slip distance (D_c), these thermally activated weakening mechanisms lead to a slip-dependent friction model with two sequential strength drops (Fig. 3).

The main goal of this work is to show that the double-slip-weakening friction in the form proposed by [Kanamori and Heaton \(2000\)](#) (Fig. 3) offers a plausible model for the rupture process of the 2011 Tohoku earthquake, including large shallow slip, rupture reactivation, and large rupture

extent. First, we present evidence supporting this friction model, obtained from seismological observations, laboratory experiments, and theoretical considerations. Then, we extend the dynamic rupture model developed by [Galvez et al. \(2014\)](#); hereafter referred to as G14) by modifying the slip-weakening friction model to account for rupture reactivation. Finally, we show that this model produces (1) a rupture pattern consistent with a kinematic source inversion model that features rupture reactivation and (2) ground-motion patterns along the Japanese coast consistent with the observations.

Evidence of Double-Slip-Weakening Friction Promoting Rupture Reactivation

The stress changes inferred from kinematic models provide constraints on frictional strength evolution during rupture (e.g., [Bouchon, 1997](#); [Ide and Takeo, 1997](#); [Dalguer et al., 2002](#)). We compute the dynamic fault stress changes implied by the [Lee et al. \(2011\)](#) kinematic source model by applying its spatiotemporal distribution of slip velocity as a boundary condition along the fault in a spectral element seismic-wave propagation simulation done with the SPEC-FEM3D code. Figure 2b, 2c, and 2d, respectively, shows

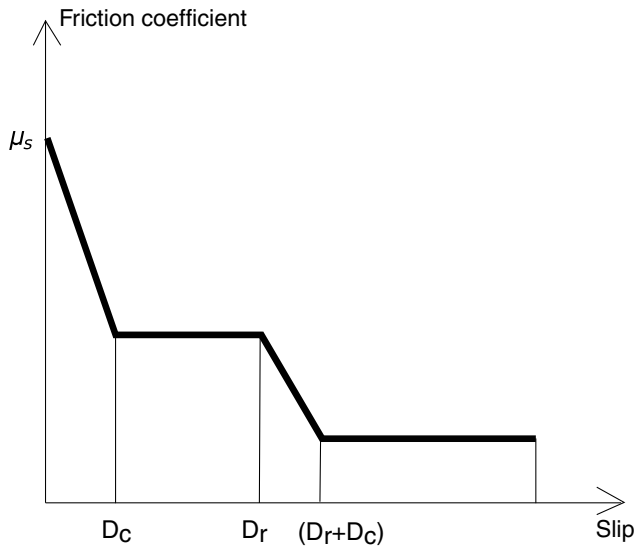


Figure 3. Slip-weakening friction model with two sequential strength drops. The second weakening phase is activated at a large slip D_r , by thermally activated physicochemical processes such as fault-zone fluid pressurization due to dehydration or decomposition reactions.

the along-dip slip velocity, slip, and computed shear stress change around the hypocenter as a function of time. The stress change features two sequential drops, correlated in time with two peaks of slip velocity. Figure 2e shows the stress change as a function of slip. The similarity with the proposed slip-weakening friction model shown in Figure 3 is remarkable. In particular, it shows that the critical slip for the onset of the second weakening is $D_r \approx 20$ m in the hypocentral region.

Additional evidence of secondary frictional weakening is found in laboratory rock experiments. Dramatic weakening is often observed in rock friction experiments at sliding velocities representative of seismic slip (~ 1 m/s) and has been attributed to thermomechanical and physicochemical processes, including flash heating, melting, and gelification, decarbonation, and dehydration reactions (e.g., Di Toro *et al.*, 2012). Han *et al.* (2007) performed experiments on calcite at seismic slip rates and found that decarbonation induces pronounced fault weakening, which they attributed to flash heating on ultrafine particles produced by thermal decomposition. The high-velocity frictional experiments of O'Hara *et al.* (2006) on bituminous coal gouge, proposed as an analog for hydrous fault zones, showed two major strength drops (see fig. 2 in O'Hara *et al.*, 2006). The second weakening occurred after 20–25 m of slip and was attributed to gouge compaction and ensuing pressurization of gas released by thermal decomposition.

Theoretical studies provide further support for a double-weakening friction model enabled by thermochemical decomposition. We first note that thermal pressurization alone produces gradual weakening (Rice, 2006), in contrast to the conceptual model by Kanamori and Heaton (2000), and that melting temperatures are not reached during earthquake slip

in rupture models that include thermal pressurization (Garagash, 2012). Sulem and Famin (2009) developed a numerical model of fault-strength evolution, including shear heating, thermal pressurization, and the mechanical effects of calcite volume loss, heat consumption, and CO_2 production. In their simulations at prescribed slip velocity, a second strength drop occurs due to additional pressurization induced by rapid decarbonation when a critical temperature of about 700°C is reached. Strengthening is subsequently caused by the increase of porosity and permeability due to the solid decomposition. Brantut *et al.* (2010) developed analytical models for strength evolution of hydrous fault zones and showed that dehydration reactions can cause a significant second weakening phase if the reaction rate is comparable or faster than the thermal pressurization process, which is favored by a thick slip zone. Further theoretical analysis of the problem was presented by Platt, Brantut, and Rice (2015) and Platt, Viesca, and Garagash (2015).

On the basis of estimates of peak temperature achieved on a fault undergoing thermal pressurization, Garagash (2012) argued that thermal decomposition could be triggered at depths larger than ~ 15 km, or ~ 6 km in a damaged fault zone. Theoretical work indicates that the occurrence and significance of weakening by thermal decomposition depends not only on fault-zone material properties, but also on background stress. Platt, Viesca, and Garagash (2015) showed that weakening by thermal decomposition becomes significant if it overcomes the strengthening effect of hydraulic diffusion; this occurs if the temperature exceeds a critical value, which they found to be higher if the background shear stress is lower. Moreover, in dynamic rupture simulations with thermal pressurization, the temperature rise is higher if background stress is larger (Noda *et al.*, 2009). This implies that, comparing fault areas of identical material properties and initial temperature, thermal decomposition weakening is favored in areas of higher stress, which can operate as asperities (large slip areas) during an earthquake, and is less expected in their surrounding, lower-stress areas.

Field evidences that mineral decomposition reactions may occur during earthquakes have been found in cores from the Chelungpu fault that hosted the 1999 Chi-Chi, Taiwan earthquake (Hirono *et al.*, 2008, 2015; Hamada *et al.*, 2009) and from the Nojima fault that hosted the 1995 Kobe, Japan, earthquake (Famin *et al.*, 2008). In particular, subduction fault gouges rich in clay minerals or phyllosilicates such as chlorite, talc, and serpentinite can host dehydration reactions at temperatures reached during earthquake slip.

Dynamic Rupture Model Parameterization

The seismological, experimental, and theoretical arguments presented in the previous discussion support the possibility of double weakening, in particular induced by thermal decomposition. However, the purpose of the present work is not to simulate or to assess the viability of a specific physical mechanism in detail. This would require the imple-

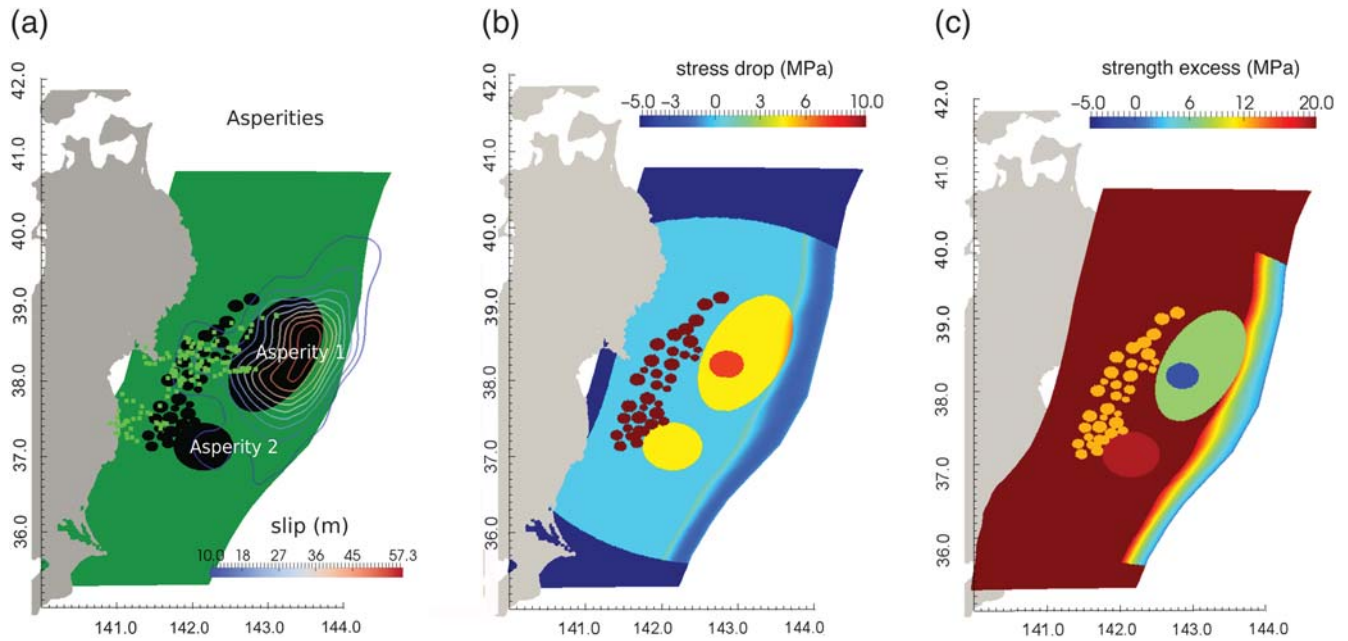


Figure 4. Dynamic rupture model setup. (a) Distribution of asperities (dark patches) comprising two large asperities constrained by kinematic source inversion models and several small deep asperities constrained by backprojection source imaging. Black curves are slip contours from the finite source inversion model by [Lee et al. \(2011\)](#). Light green points are high-frequency radiation locations from the [Meng et al. \(2011\)](#) backprojection source imaging. (b) Nominal stress drop, defined as (initial along-dip shear stress) – (dynamic friction coefficient) \times (initial normal stress). (c) Nominal strength excess, defined as (static friction coefficient) \times (initial normal stress) – (initial along-dip shear stress).

mentation of coupled thermohydrochemical processes in a 3D rupture-dynamics simulation code. It would also require efforts to constrain the relevant fault-zone parameters and to evaluate the effect of their (often large) uncertainties. Instead, our goal is to demonstrate conceptually, through simulations based on a phenomenological slip-weakening friction law, that the assumption of double weakening is consistent with basic rupture and ground-motion patterns.

We extend the model developed by G14 to account for rupture reactivation. G14 developed an asperity model to simulate the dynamic rupture process of the 2011 Tohoku earthquake, in particular to reproduce qualitatively the observed depth-dependent frequency content of seismic radiation and large slip close to the trench. The model included a nonplanar megathrust fault geometry adapted from [Simons et al. \(2011\)](#). The unstructured mesh-generation software CUBIT was utilized to create a spectral element mesh accounting for these geometrical complexities. Our simulations employ the unstructured spectral element code SPEC3D (Peter et al., 2011), in which G14 implemented dynamic rupture capabilities to enable accurate simulations of dynamic rupture and seismic-wave propagation. G14 demonstrated the stability and accuracy of SPEC3D for dynamic rupture simulations in the subduction wedge geometry of Tohoku. In particular, results of spatial resolution tests presented in appendix A of G14 show that the rupture process is accurately resolved with an average grid size of 500 m on the fault, a value we also adopt in the present model (i.e., fourth-order spectral elements of size 2000 m). In that test, decreasing

the average grid size to 125 m (fourth-order spectral elements of size 500 m) provided similar results.

The G14 model is composed of two large asperities (1 and 2) and a collection of small circular asperities in deeper regions, as shown in Figure 4. The location of the two main asperities corresponds approximately to the large shallow slip inferred from low-frequency (LF) data through kinematic source inversions (e.g., [Lee et al., 2011](#); [Suzuki et al., 2011](#); [Yagi and Fukahata, 2011](#); [Yoshida, 2011](#); [Yue and Lay, 2011](#); [Wei et al., 2012](#)). The small asperities are placed in the general areas of high-frequency (HF) radiation identified by backprojection techniques (e.g., [Ishii, 2011](#); [Meng et al., 2011](#); [Simons et al., 2011](#); [Roten et al., 2012](#); [Yagi et al., 2012](#)). Figure 4a compares the location of the asperities with the final slip model of [Lee et al. \(2011\)](#), denoted with contour lines, and with the HF radiation points (green circles) obtained by [Meng et al. \(2011\)](#). The largest asperity (asperity 1) was defined as an ellipse that delimits the region of large slip inferred by [Lee et al. \(2011\)](#). The depth dependency of LF and HF radiation implied by this rupture model was presented by G14, and other studies based on asperity models were developed by [Aochi and Ide \(2011, 2014\)](#), [Huang et al. \(2013, 2014\)](#), and [Ide and Aochi \(2013\)](#). The shallow zone of megathrusts is characterized by velocity strengthening friction due to the presence of sediments in the fault zone (e.g., [Marone and Scholz, 1988](#); [Oleskevich et al., 1999](#)). To approximately mimic this mechanism, we impose a negative stress drop at shallow depth (e.g., [Dalguer et al., 2008](#); [Pitarka et al., 2009](#)).

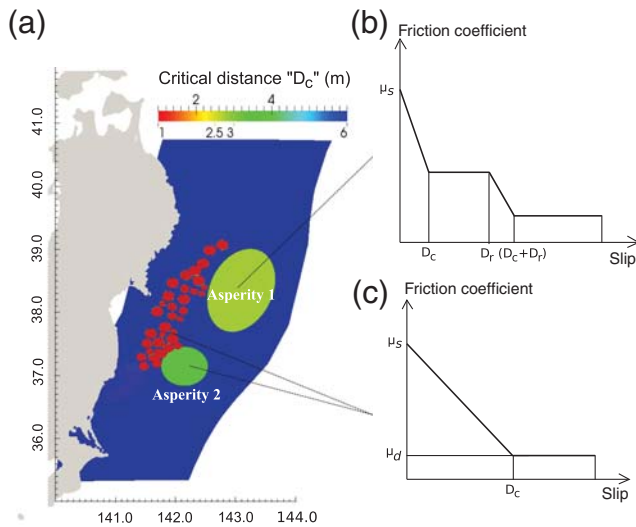


Figure 5. Dynamic rupture model setup (continued). (a) Assumed distribution of slip-weakening critical distance D_c . (b) The largest asperity is governed by the double-slip-weakening friction law (Figs. 2e and 3). (c) The rest of the fault is governed by the conventional linear slip-weakening friction law.

Here, we extend the G14 model to account for rupture reactivation by incorporating the double-slip-weakening friction shown in Figure 3. The rupture in the largest asperity is governed by our proposed double-slip-weakening friction. This asperity breaks with two sequential stress drops, each of 4.5 MPa, resulting in a total stress drop of 9 MPa. In the rest of the fault, where initial stresses are lower, rupture is governed by the standard linear slip-weakening friction model (Andrews, 1976). The distributions of (1) nominal stress drop, defined as (initial along-dip shear stress) – (dynamic friction coefficient) \times (initial normal stress), (2) nominal strength excess, defined as (static friction coefficient) \times (initial normal stress) – (initial along-dip shear stress), and (3) critical slip distance (shown in Figs. 4b, 4c, and 5, respectively) were obtained by a systematic tuning of the dynamic parameters (initial stresses, friction coefficients, and D_c) to qualitatively fit the kinematic source model of Lee *et al.* (2011) and the observed ground-motion pattern shown in Figure 1. The blue and red regions of Figure 4b and 4c represent the artificial nucleation patch, where the static coefficient is slightly reduced so that the initial yield strength, defined as (static friction coefficient) \times (initial normal stress), is slightly below the initial along-dip shear stress. We adopt the 1D layered velocity structure of Fukuyama *et al.* (1998) (Table 1).

Results

Fault Rupture

Our dynamic rupture model generates a rupture reactivation process consistent with the one observed in the kinematic source model of Lee *et al.* (2011). Snapshots of the simulated slip rate are shown in Figure 6. An initial rupture

Table 1
1D Velocity Structure

Thickness (km)	P-Wave Velocity (km/s)	S-Wave Velocity (km/s)	Density (kg/m ³)
3	5.5	3.14	2300
15	6.0	3.55	2400
15	6.7	3.83	2800
67	7.8	4.46	3200
∞	8.0	4.57	3300

front propagates up-dip, with subshear speed, and reaches the trench at $t \approx 35$ s (time is relative to the rupture onset), breaking a small portion of it. Simultaneously, the rupture also propagates down-dip, although slowly, and starts to break the closest deep small asperities. Hereafter, we refer to this first episode as phase 1. At $t \approx 40$ s, a new episode initiates with an energetic rupture reactivation around the hypocenter (phase 2). To better illustrate this, in Figure 7 we show the spatiotemporal evolution of slip velocity along the longitudinal transect passing through the hypocenter (indicated as section PQ in the first snapshot of Fig. 6). Similar to the kinematic source model of Lee *et al.* (2011) (Fig. 2a), two sets of rupture fronts emerge from the hypocenter area, corresponding to phases 1 and 2 (black lines). During phase 2, the new rupture front propagates both up-dip and down-dip. The upward front propagates with supershear speed, reaches the trench at $t \approx 50$ s, and then propagates bilaterally along strike. The downward rupture propagates with subshear speed, penetrates the deepest region, and generates high peak-slip velocities when it breaks the small asperities. These sharp peak-slip velocities are expected to radiate at the high frequencies imaged by backprojection studies but remain unresolved in lower-frequency kinematic source models (Fig. 2a). At $t \approx 80$ s, the deep rupture front starts propagating southward, then travels slowly a few kilometers until it reaches the second big asperity (asperity 2) at $t \approx 100$ s. Then a third episode initiates, leading to the complete rupture of asperity 2 (phase 3). The whole rupture stops in the southern part at $t \approx 160$ s.

The final slip distributions resulting from our dynamic model and from the kinematic model of Lee *et al.* (2011) are compared in Figure 8. The locations of the maximum slip area are consistent in both models.

Seismic-Wave Propagation

Inspection of the simulated ground-velocity wavefield and comparison with the distinct rupture phases (Figs. 6 and 7) reveal the correspondence between the rupture process and the prominent wave groups arriving to the Japanese coast. The seismic waves are well resolved by our simulation up to 0.2 Hz. $\text{\textcircled{E}}$ The movie, available in the electronic supplement to this article, shows in detail the evolution of the east–west ground velocity, filtered in the 0.01–0.05 Hz frequency range to highlight the main groups of waves. Four selected snapshots of ground velocity are shown in Figure 9a,

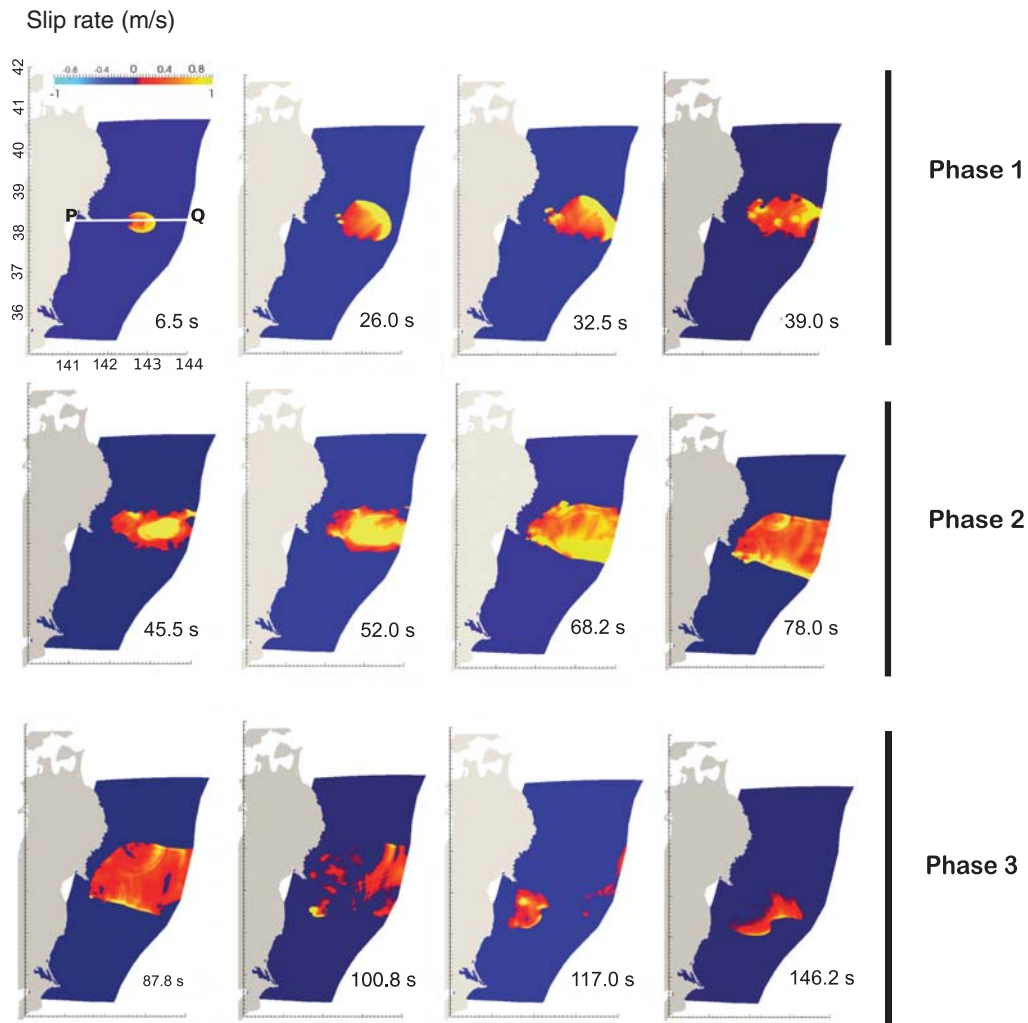


Figure 6. Dynamic rupture simulation results and identification of three rupture phases. Distribution of slip rate at representative times of three rupture phases: initial rupture of the main asperity (phase 1), rupture reactivation of the main asperity (phase 2), and rupture of the second large asperity (phase 3).

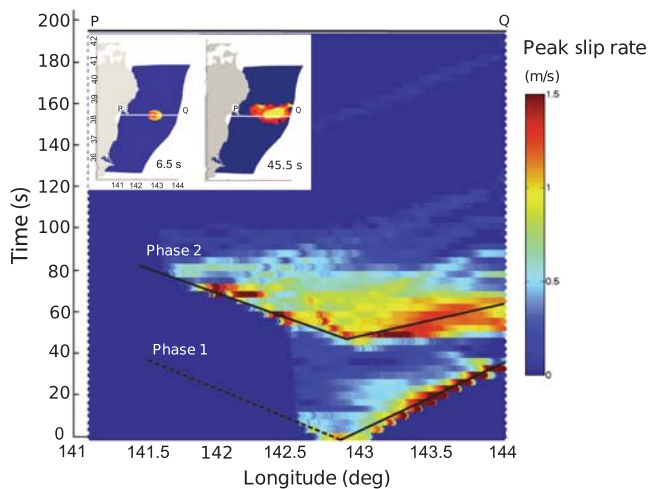


Figure 7. Spatiotemporal evolution of the slip rate along the cross section PQ through the hypocenter indicated in the upper left corner inset. Black lines indicate the rupture reactivation phases 1 and 2, as in Figure 2a.

along with simulated seismograms (Fig. 9b) at the locations of the K-NET and KiK-net seismic stations distributed along the Japanese coast (indicated by white squares in Fig. 9a). Three prominent wave groups are identified. The first group arrives at the Japanese coast between 50 and 65 s and corresponds to the waves radiated from phase 1 of the rupture. The second group of waves reaches the coast between 90 and 100 s and is attributed to radiation from the rupture reactivation during phase 2 of the rupture. The third group of waves hits the coast of the Ibaraki region at about 120 s and is associated with the rupture of the southern asperity during phase 3.

These three groups of waves resemble the S1, S2, and S3 wavefronts identified in the observed ground motions (Fig. 1). The left and middle panels of Figure 10 show, respectively, simulated and observed ground velocities at the selected K-NET and KiK-net stations. Their similarity is remarkable, suggesting that our dynamic rupture model with rupture reactivation explains the ground-motion pattern

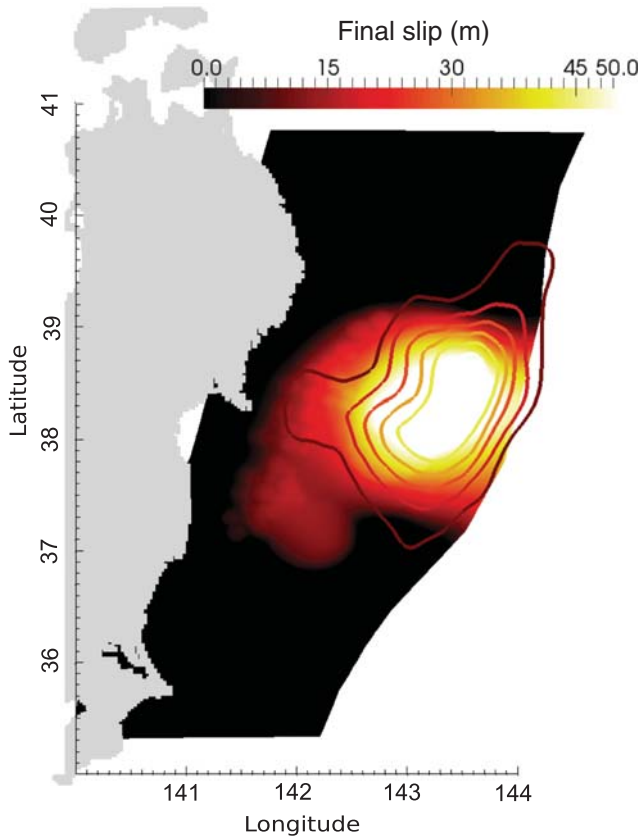


Figure 8. Comparison of final slip distribution from our dynamic rupture model (background colors) and from the Lee *et al.* (2011) kinematic source model (colored contours).

recorded in the Tohoku earthquake. As a reference, the right panel of Figure 10 shows the ground velocities generated by the dynamic model of G14, which does not include rupture reactivation. This model does not reproduce clearly separated wavefronts S1 and S2, but generates a single S2 front with larger amplitudes and longer duration than those observed, because the entire stress drop (9 MPa) in asperity 1 is released at once.

In Figure 11, we compare the three components of simulated and observed ground velocities at three representative KiK-net stations located onshore of the north (IWTH20), middle (MYGH08), and south (IBR002) portions of the rupture of the model with reactivation and model G14 without reactivation. The seismograms are low-pass filtered with a frequency cutoff of 0.2 Hz. In general, synthetics of our model with reactivation follow the waveform patterns of observations better than those of the G14 model. The best agreement is achieved at the middle station (MYGH08) and the worse at the southern station (IBR002). Waveform shapes and amplitudes in the horizontal components agree better than in the vertical component.

We also compare the ground displacements simulated by our model with rupture reactivation (Fig. 12a) and by model G14 without reactivation (Fig. 12b) to the observed continuous GPS data recorded along the Japanese coast (east–west

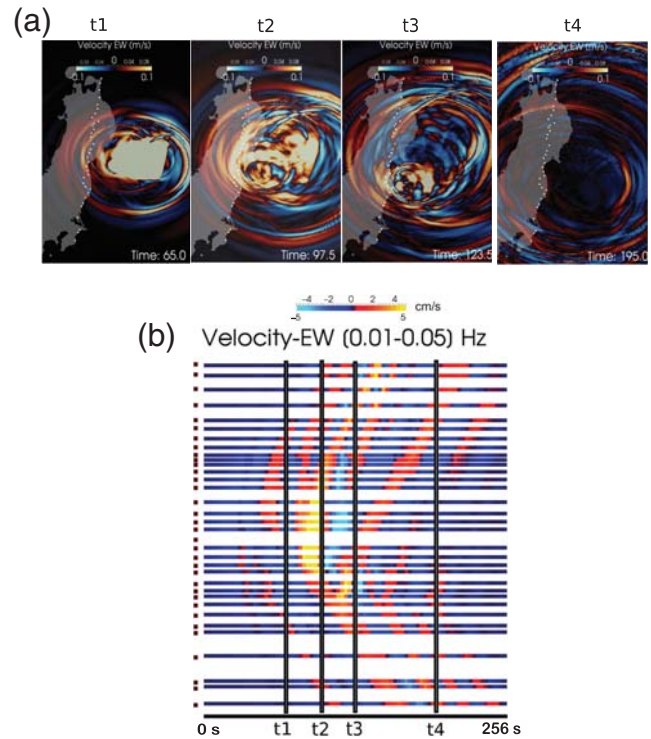


Figure 9. Wavefield radiated by our dynamic rupture model with rupture reactivation. (a) Snapshots of east–west ground velocities (times are labeled in the bottom right corners) and (b) velocity traces (amplitudes represented by colors) at selected K-NET and KiK-net seismic stations along the Japanese coast (white squares). Each vertical solid black line corresponds to the snapshot time shown in (a).

component). Only our model with reactivation shows good consistency with the observed displacements, in shape and amplitude. In particular, it reproduces the three main groups of waves that are also observed in the GPS data (Fig. 1). As shown in Figure 12a, our model with rupture reactivation better explains the displacements at stations located in the middle latitude of the rupture (Miyagi and Fukushima areas) where the two groups of waves S1 and S2 are radiated (according to our model) from the repeated rupture of asperity 1.

These comparisons suggest that the two episodes of stress drop leading to rupture reactivation are needed to reproduce the observed ground-motion pattern.

Rupture Reactivation and Small Asperities Enabled the M_w 9 Event

In the framework of our dynamic model, we investigate the role of rupture reactivation and deep small asperities in enabling the Tohoku earthquake to reach its final magnitude, M_w 9. For this purpose, results of three dynamic rupture models are compared (Fig. 13a). Model A is the dynamic rupture model with rupture reactivation in asperity 1 (two stress drops of 4.5 MPa each) and multiple small asperities at greater depth. Model B is identical to model A but without rupture reactivation (asperity 1 has a single stress drop of

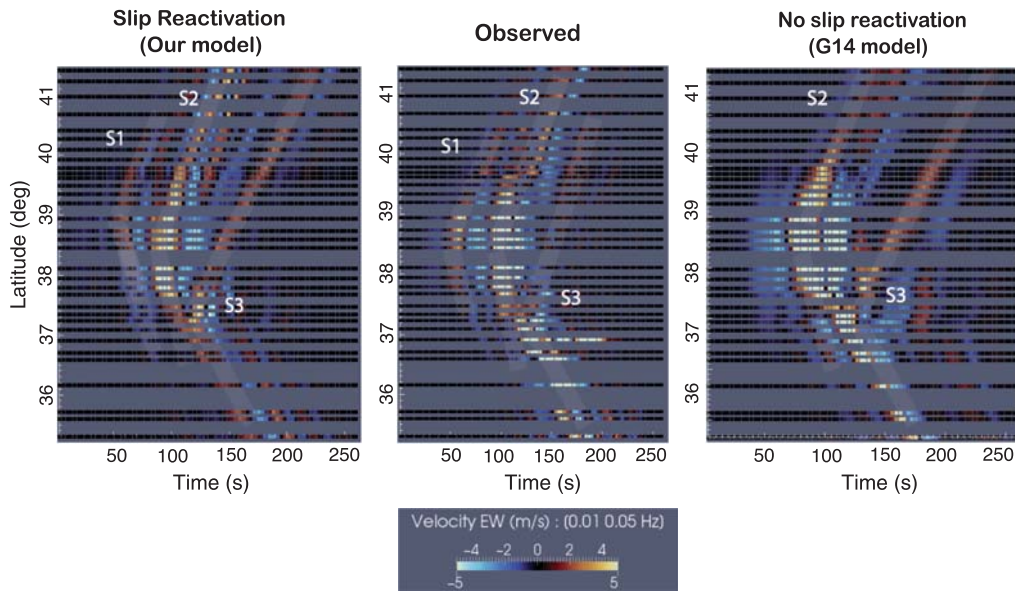


Figure 10. Velocity traces at the selected seismic stations, filtered from 0.01 to 0.05 Hz, from (left) our dynamic rupture model with rupture reactivation, (middle) the observed strong-motion data, and (right) the *Galvez et al. (2014)* dynamic rupture model without rupture reactivation.

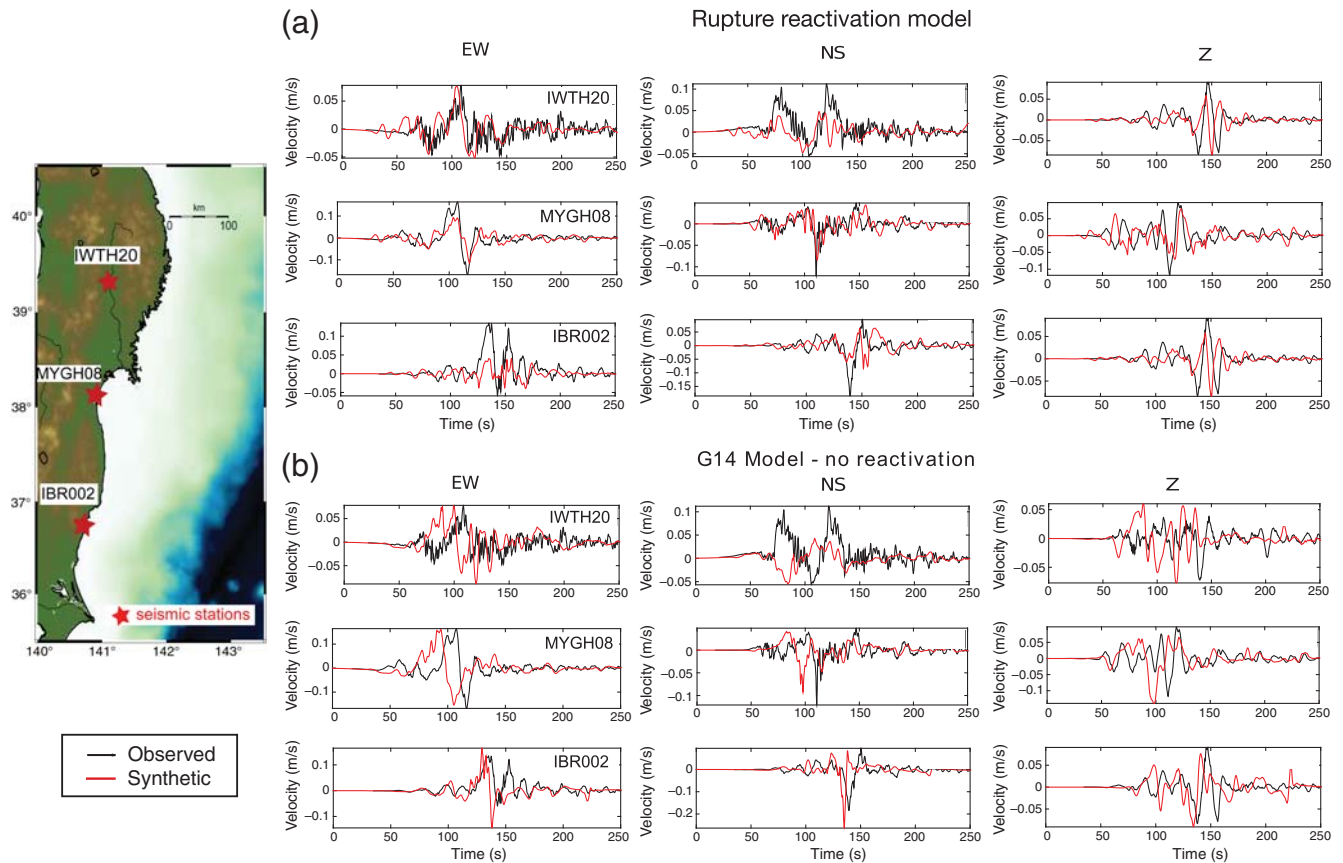


Figure 11. Comparison of three-component ground-velocity time series, low-pass filtered up to 0.2 Hz, recorded by three KiK-net stations (IWTH20, MYGH08, and IBR002; their locations are shown in the map on the left) and computed by (a) our dynamic rupture model with rupture reactivation and (b) the *Galvez et al. (2014)* model without rupture reactivation.

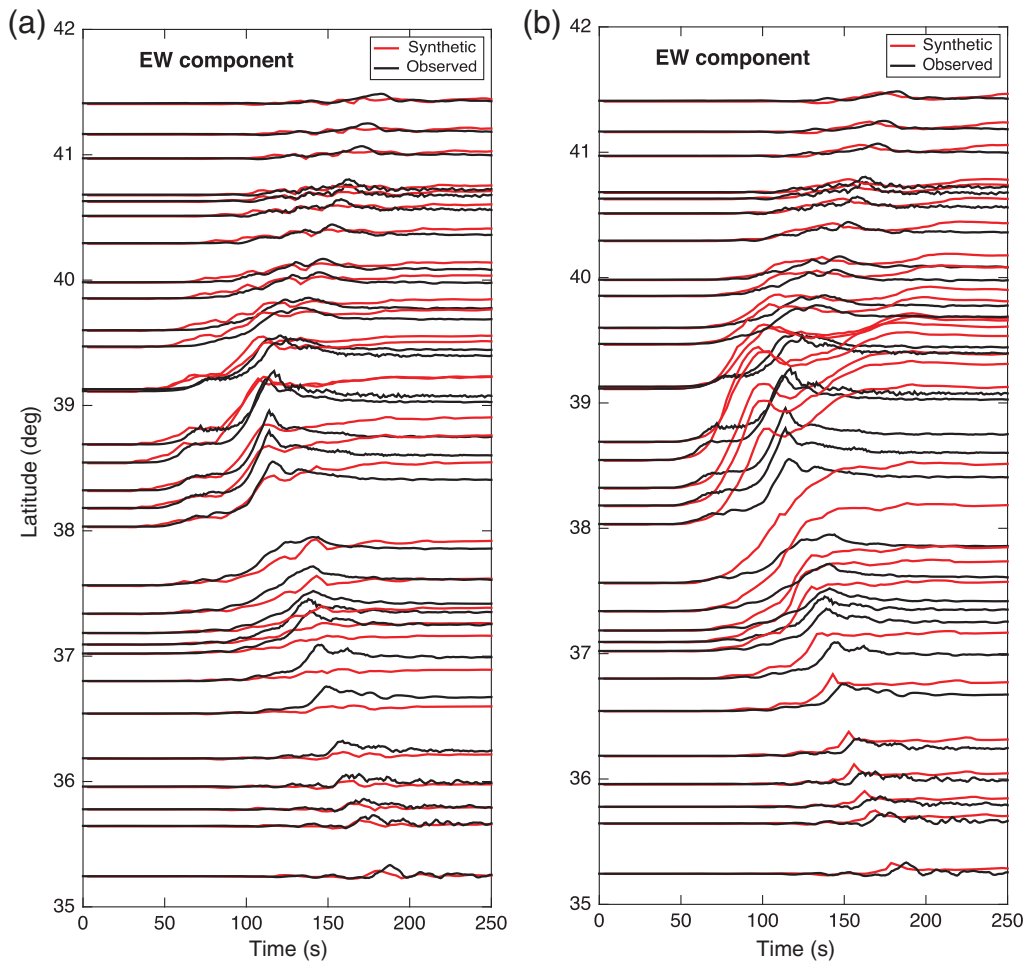


Figure 12. Comparison of east–west displacement time histories recorded by GPS GEONET stations along the Japanese coast with those obtained from (a) our dynamic rupture model with rupture reactivation and (b) the Galvez *et al.* (2014) model without rupture reactivation. For clarity, time series are vertically offset according to their latitude.

4.5 MPa). Model C is identical to model A but with the small asperities removed.

Model B produces an M_w 8.6 earthquake, which breaks only the small asperities located just below asperity 1 and leaves the second large asperity unbroken. Model C produces an M_w 8.75 event, again without breaking asperity 2. Figure 13b shows the final slip distribution of each model. Maximum slip values are around 50, 20, and 40 m, respectively, for models A, B, and C. The slip of models B and C spans an area confined to the vicinity of asperity 1. Figure 13c shows the seismic moment rates of each model. Our preferred model, model A, generates three pulses in the seismic moment rate, corresponding to the three rupture phases described previously (see Figs. 6 and 7) and to the three wave groups identified in Figures 1 and 9. Model B generates only the first pulse (phase 1), with amplitude slightly lower than the one produced by model A. Model C generates only the first and second pulses (phases 1 and 2) and the latter, caused by rupture reactivation, is smaller (about one-third) than in model A.

These model comparisons suggest that both the lack of rupture reactivation (model B) and the absence of small asper-

ities (model C) cause the down-dip rupture to die out earlier, limiting the rupture area and final magnitude of the earthquake. The series of deep small asperities serves as a bridge to connect the rupture of asperities 1 and 2, which enhances the accumulation of slip close to the trench and enables rupture growth up to an M_w 9.0 event. In the context of our study, both rupture reactivation and deep small asperities are necessary to generate a megathrust event of a size consistent with observations.

Conclusions

We developed a 3D dynamic model of the rupture process of the 2011 Tohoku earthquake that includes the rupture reactivation phenomenon (repeated nucleation of rupture in the hypocentral area) previously inferred from seismological observations. Our model features a slip-weakening friction with two sequential strength drops, supported by the evolution of dynamic stresses derived from a finite source inversion model and by laboratory experiments involving thermochemical weakening mechanisms associated with mineral decomposition reactions.

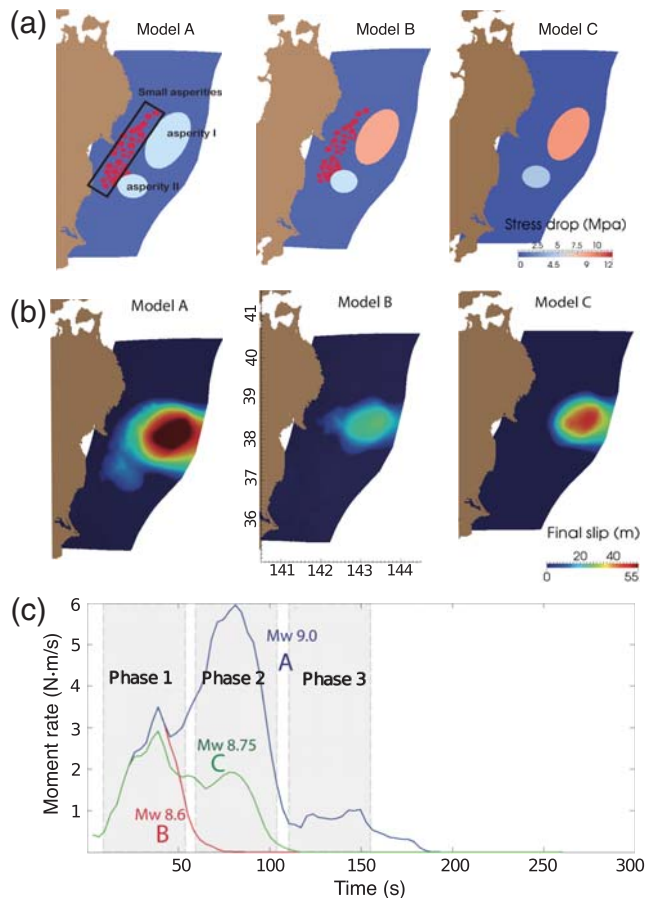


Figure 13. Comparison of first-order source properties from three dynamic rupture models. Model A is our primary dynamic rupture model with rupture reactivation (Figs. 4 and 5). Model B is a variant of model A without rupture reactivation (stress drop is 4.5 MPa in the main asperity). Model C is a variant of model A without small deep asperities. For each model we show (a) asperity distribution, (b) final slip distribution, and (c) moment rate function. Vertical gray bands in (c) indicate the three rupture phases identified in Figure 6.

Three prominent groups of seismic waves observed in ground motions recorded along the Japanese coast are generated in our model by three notable rupture phases. The first two originate from the main asperity, which contains the hypocenter and experiences rupture reactivation. The third rupture phase involves a second large asperity located in the southern portion of the rupture. The ground velocity and displacement waveforms recorded by the K-NET and KiK-net strong-motion networks and the GEONET GPS network are generally reproduced by our numerical simulation. These results show that a friction model with rupture reactivation can explain the complex dynamic rupture process of the 2011 Tohoku earthquake and the observed ground-motion patterns near the source.

Our dynamic model has two main ingredients, rupture reactivation of the main asperity and the presence of deep small asperities. The latter were previously found to explain the enhanced high-frequency radiation in the deeper portions

of the Tohoku earthquake rupture zone, as revealed by teleseismic backprojection source imaging. Here, we found that both ingredients may have played a crucial role in enabling the large size of this megathrust rupture. Our modeling results suggest that the small asperities serve as a bridge to connect the rupture of the hypocentral asperity to that of the southern asperity; however, without rupture reactivation in the first asperity, this bridge is not activated.

The additional strength drop caused by decomposition reactions triggered by shear heating can significantly enhance the final rupture size and rupture complexity of large earthquakes.

Data and Resources

The strong ground motion data used in this work are from the K-NET and KiK-net database (<http://www.kyoshin.bosai.go.jp>, last accessed November 2013) and the Global Positioning System (GPS) records are from the GNSS Earth Observation Network System (GEONET) of Japan, operated by the Geospatial Information Authority of Japan (GSI; <http://www.gsi.go.jp/ENGLISH/index.html>, last accessed November 2013).

Acknowledgments

This study was supported by the Quantitative Estimation of Earth's Seismic Sources and Structure (QUEST) project funded by the Seventh Framework Programme of the European Commission, the Advanced Simulation of Coupled Earthquake and Tsunami Events (ASCETE) Project funded by the Volkswagen Foundation within the program “New Conceptual Approaches to Modeling and Simulation of Complex Systems,” and National Science Foundation (NSF) CAREER Award EAR-1151926. We thank the Swiss project “High-Rate GNSS for Seismology,” funded by the Swiss National Foundation, for providing us with the Global Positioning System (GPS) records of the GNSS Earth Observation Network System (GEONET). Simulations were done at the Swiss National Supercomputing Center (CSCS), under the production projects “Development of Dynamic Rupture Models to Study the Physics of Earthquakes and Near-Source Ground Motion” and “Development of a Database of Physics-Based Synthetic Earthquakes for Ground Motion Prediction.”

References

- Andrews, D. J. (1976). Rupture velocity of plane-strain shear cracks, *J. Geophys. Res.* **81**, 5679–5687.
- Aochi, H., and S. Ide (2011). Conceptual multi-scale dynamic rupture model for the 2011 Tohoku earthquake, *Earth Planets Space* **63**, 761–765.
- Aochi, H., and S. Ide (2014). Ground motions characterized by a multi-scale heterogeneous earthquake model, *Earth Planets Space* **66**, no. 1, 1–12.
- Bouchon, M. (1997). The state of stress on some faults of the San Andreas system as inferred from near-field strong motion data, *J. Geophys. Res.* **102**, 11,731–11,744.
- Brantut, N., A. Schubnel, J. Corvisier, and J. Sarout (2010). Thermochemical pressurization of faults during coseismic slip, *J. Geophys. Res.* **115**, no. B5, 2156–2202.
- Cubas, N., N. Lapusta, J. P. Avouac, and H. Perfettini (2015). Numerical modeling of long-term earthquake sequences on the NE Japan megathrust: Comparison with observations and implications for fault friction, *Earth Planet. Sci. Lett.* **419**, 187–198.
- Dalguer, L. A., K. Irikura, J. D. Riera, and H. C. Chiu (2001a). Fault dynamic rupture simulation of the hypocenter area of the thrust fault of

- the 1999 Chi-Chi (Taiwan) earthquake, *Geophys. Res. Lett.* **28**, no. 7, 1327–1330.
- Dalguer, L. A., K. Irikura, J. D. Riera, and H. C. Chiu (2001b). The importance of the dynamic source effects on strong ground motion during the 1999 Chi-Chi, Taiwan, earthquake: Brief interpretation of the damage distribution on buildings, *Bull. Seismol. Soc. Am.* **91**, no. 5, 1112–1127.
- Dalguer, L. A., K. Irikura, W. Zhang, and J. D. Riera (2002). Distribution of dynamic and static stress changes during 2000 Tottori (Japan) earthquake: Brief interpretation of the earthquake sequences; foreshocks, mainshock and aftershocks, *Geophys. Res. Lett.* **29**, no. 16, 1758, doi: [10.1029/2001GL014333](https://doi.org/10.1029/2001GL014333).
- Dalguer, L. A., H. Miyake, S. M. Day, and K. Irikura (2008). Surface rupturing and buried dynamic rupture models calibrated with statistical observations of past earthquakes, *Bull. Seismol. Soc. Am.* **98**, 1147–1161, doi: [10.1785/0120070134](https://doi.org/10.1785/0120070134).
- Di Toro, G., R. Han, T. Hirose, N. De Paola, S. Nielsen, K. Mizoguchi, F. Ferri, M. Cocco, and T. Shimamoto (2012). Fault lubrication during earthquakes, *Nature* **471**, no. 7339, 494–498.
- Famin, V., S. Nakashima, A.-M. Boullier, K. Fujimoto, and T. Hirono (2008). Earthquakes produce carbon dioxide in crustal faults, *Earth Planet. Sci. Lett.* **265**, 487–497.
- Fukuyama, E., M. Ishida, D. S. Dreger, and H. Kawai (1998). Automated seismic moment tensor determination by using on-line broadband seismic waveforms, *Zisin* **51**, 149–156.
- Gabriel, A. A., J. P. Ampuero, L. A. Dalguer, and P. M. Mai (2012). The transition of dynamic rupture styles in elastic media under velocity-weakening friction, *J. Geophys. Res.* **117**, no. B09311, doi: [10.1029/2012JB009468](https://doi.org/10.1029/2012JB009468).
- Galvez, P., J. P. Ampuero, L. A. Dalguer, S. N. Somala, and T. Nissen-Meyer (2014). Dynamic earthquake rupture modelled with an unstructured 3-D spectral element method applied to the 2011 M9 Tohoku earthquake, *Geophys. J. Int.* **198**, no. 2, 1222–1240.
- Garagash, D. I. (2012). Seismic and aseismic slip pulses driven by thermal pressurization of pore fluid, *J. Geophys. Res.* **117**, no. B04314, doi: [10.1029/2011JB008889](https://doi.org/10.1029/2011JB008889).
- Goto, H., Y. Yamamoto, and S. Kita (2012). Dynamic rupture simulation of the 2011 Off the Pacific Coast of Tohoku earthquake: Multi-event generation within dozens of seconds, *Earth Planets Space* **64**, no. 12, 1167–1175.
- Hamada, Y., T. Hirono, W. Tanikawa, W. Soh, and S. Song (2009). Energy taken up by co-seismic chemical reactions during a large earthquake: An example from the 1999 Taiwan Chi-Chi earthquake, *Geophys. Res. Lett.* **36**, L06301, doi: [10.1029/2008GL036772](https://doi.org/10.1029/2008GL036772).
- Han, R., T. Shimamoto, T. Hirose, J. H. Ree, and J. I. Ando (2007). Ultralow friction of carbonate faults caused by thermal decomposition, *Science* **316**, no. 5826, 878–881.
- Hirono, T., K. Fujimoto, T. Yokoyama, Y. Hamada, W. Tanikawa, O. Tadai, T. Mishima, M. Tanimizu, W. Lin, W. Soh, *et al.* (2008). Clay mineral reactions caused by frictional heating during an earthquake: An example from the Taiwan Chelungpu fault, *Geophys. Res. Lett.* **35**, no. 16, L16303, doi: [10.1029/2008GL034476](https://doi.org/10.1029/2008GL034476).
- Hirono, T., Y. Maekawa, and H. Yabuta (2015). Investigation of the records of earthquake slip in carbonaceous materials from the Taiwan Chelungpu fault by means of infrared and Raman spectroscopies, *Geochem. Geophys. Geosyst.* **16**, no. 5, 1233–1253, doi: [10.1002/2014GC005622](https://doi.org/10.1002/2014GC005622).
- Honda, R., Y. Yukutake, H. Ito, M. Harada, T. Aketagawa, A. Yoshida, S. Sakai, S. Nakagawa, N. Hirata, K. Obara, and H. Kimura (2011). A complex rupture image of the 2011 Off the Pacific Coast of Tohoku earthquake revealed by the MeSO-net, *Earth Planets Space* **63**, no. 7, 583–588.
- Huang, Y., J. P. Ampuero, and H. Kanamori (2014). Slip-weakening models of the 2011 Tohoku-Oki earthquake and constraints on stress drop and fracture energy, *Pure Appl. Geophys.* **171**, no. 10, 2555–2568.
- Huang, Y., L. Meng, and J. P. Ampuero (2013). A dynamic model of the frequency-dependent rupture process of the 2011 Tohoku-Oki earthquake, *Earth Planets Space* **64**, no. 12, 1061–1066.
- Ide, S., and H. Aochi (2013). Historical seismicity and dynamic rupture process of the 2011 Tohoku-Oki earthquake, *Tectonophysics* **600**, 1–13.
- Ide, S., and M. Takeo (1997). Determination of constitutive relations of fault slip based on seismic waves analysis, *J. Geophys. Res.* **102**, 27,379–27,391.
- Ide, S., A. Baltay, and G. C. Beroza (2011). Shallow dynamic overshoot and energetic deep rupture in the 2011 M_w 9.0 Tohoku-Oki earthquake, *Science* **332**, 1426–1429, doi: [10.1126/science.1207020](https://doi.org/10.1126/science.1207020).
- Ishii, M. (2011). High-frequency rupture properties of the M_w 9.0 Off the Pacific Coast of Tohoku earthquake, *Earth Planets Space* **63**, 609–614, doi: [10.5047/eps.2011.07.009](https://doi.org/10.5047/eps.2011.07.009).
- Kanamori, H., and T. Heaton (2000). Microscopic and macroscopic physics of earthquakes, in *Geocomplexity and the Physics of Earthquakes*, J. B. Rundle, D. L. Turcotte, and W. Klein (Editors), American Geophysical Monograph, Vol. 120, 1–17, doi: [10.1029/GM120](https://doi.org/10.1029/GM120).
- Kaneko, Y., J. P. Avouac, and N. Lapusta (2010). Towards inferring earthquake patterns from geodetic observations of interseismic coupling, *Nat. Geosci.* **3**, no. 5, 363–369.
- Koketsu, K., Y. Yokota, N. Nishimura, Y. Yagi, S. Miyazaki, K. Satake, Y. Fujii, H. Miyake, S. Sakai, Y. Yamanaka, and T. Okada (2011). A unified source model for the 2011 Tohoku earthquake, *Earth Planet. Sci. Lett.* **31**, 480–487, doi: [10.1016/j.epsl.2011.09.009](https://doi.org/10.1016/j.epsl.2011.09.009).
- Kozdon, J. E., and E. M. Dunham (2013). Rupture to the trench: Dynamic rupture simulations of the 11 March 2011 Tohoku earthquake, *Bull. Seismol. Soc. Am.* **103**, no. 2B, 1275–1289.
- Lee, S.-J., B.-S. Huang, M. Ando, H.-C. Chiu, and J.-H. Wang (2011). Evidence of large scale repeating slip during the 2011 Tohoku-Oki earthquake, *Geophys. Res. Lett.* **38**, no. 19, L19306, doi: [10.1029/2011GL049580](https://doi.org/10.1029/2011GL049580).
- Ma, S., and E. T. Hirakawa (2013). Dynamic wedge failure reveals anomalous energy radiation of shallow subduction earthquakes, *Earth Planet. Sci. Lett.* **375**, 113–122.
- Marone, C., and C. H. Scholz (1988). The depth of seismic faulting and the upper transition from stable to unstable slip regimes, *Geophys. Res. Lett.* **15**, 621–624.
- Meng, L., A. Inbal, and J. P. Ampuero (2011). A window into the complexity of the dynamic rupture of the 2011 M_w 9 Tohoku-Oki earthquake, *Geophys. Res. Lett.* **38**, L00G07, doi: [10.1029/2011GL048118](https://doi.org/10.1029/2011GL048118).
- Mitsui, Y., Y. Iio, and Y. Fukahata (2012). A scenario for the generation process of the 2011 Tohoku earthquake based on dynamic rupture simulation: Role of stress concentration and thermal fluid pressurization, *Earth Planets Space* **64**, no. 12, 1177–1187.
- Mitsui, Y., N. Kato, Y. Fukahata, and K. Hirahara (2012). Megaquake cycle at the Tohoku subduction zone with thermal fluid pressurization near the surface, *Earth Planet. Sci. Lett.* **325**, 21–26.
- Noda, H., and N. Lapusta (2013). Stable creeping fault segments can become destructive as a result of dynamic weakening, *Nature* **493**, no. 7433, 518–521.
- Noda, H., E. M. Dunham, and J. R. Rice (2009). Earthquake ruptures with thermal weakening and the operation of major faults at low overall stress levels, *J. Geophys. Res.* **114**, no. B07302, doi: [10.1029/2008JB006143](https://doi.org/10.1029/2008JB006143).
- O'Hara, K., K. Mizoguchi, T. Shimamoto, and J. C. Hower (2006). Experimental frictional heating of coal gouge at seismic slip rates: Evidence for devolatilization and thermal pressurization of gouge fluids, *Tectonophysics* **424**, nos. 1/2, 109–118.
- Oleskevich, D. A., R. D. Hyndman, and K. Wang (1999). The updip and downdip limits to great subduction earthquakes: Thermal and structural models of Cascadia, south Alaska, SW Japan, and Chile, *J. Geophys. Res.* **104**, no. B7, 14,965–14,991, doi: [10.1029/1999JB900060](https://doi.org/10.1029/1999JB900060).
- Peter, D., D. Komatitsch, Y. Luo, R. Martin, N. Le Goff, E. Casarotti, P. Le Loher, F. Magnoni, Q. Liu, C. Blitz, *et al.* (2011). Forward and adjoint simulations of seismic wave propagation on fully unstructured hexahedral meshes, *Geophys. J. Int.* **186**, 721–739.
- Pitarka, A., L. A. Dalguer, S. M. Day, P. Somerville, and K. Dan (2009). Numerical study of ground motion differences between buried and

- surface-rupturing earthquakes, *Bull. Seismol. Soc. Am.* **99**, no. 3, 1521–1537, doi: [10.1785/0120080193](https://doi.org/10.1785/0120080193).
- Platt, J. D., N. Brantut, and J. R. Rice (2015). Strain localization driven by thermal decomposition during seismic shear, *J. Geophys. Res.* **120**, no. 6, 4405–4433, doi: [10.1002/2014JB011493](https://doi.org/10.1002/2014JB011493).
- Platt, J. D., R. C. Viesca, and D. I. Garagash (2015). Steadily propagating slip pulses driven by thermal decomposition, *J. Geophys. Res.* **120**, no. 9, 6558–6591, doi: [10.1002/2015JB012200](https://doi.org/10.1002/2015JB012200).
- Rice, J. R. (2006). Heating and weakening of faults during earthquake slip, *J. Geophys. Res.* **111**, no. B5, B05311, doi: [10.1029/2005JB004006](https://doi.org/10.1029/2005JB004006).
- Roten, D., H. Miyake, and K. Koketsu (2012). A Rayleigh wave back-projection method applied to the 2011 Tohoku earthquake, *Geophys. Res. Lett.* **39**, L02302, doi: [10.1029/2011GL050183](https://doi.org/10.1029/2011GL050183).
- Simons, M., S. E. Minson, A. Sladen, F. Ortega, J. Jiang, S. E. Owen, L. Meng, J.-P. Ampuero, S. Wei, R. Chu, *et al.* (2011). The 2011 magnitude 9.0 Tohoku-Oki earthquake: Mosaicking the megathrust from seconds to centuries, *Science* **332**, 1421–1425.
- Sulem, J., and V. Famin (2009). Thermal decomposition of carbonates in fault zones: Slip-weakening and temperature-limiting effects, *J. Geophys. Res.* **114**, no. B3, doi: [10.1029/2008JB006004](https://doi.org/10.1029/2008JB006004).
- Suzuki, W., S. Aoi, H. Sekiguchi, and T. Kunugi (2011). Rupture process of the 2011 Tohoku-Oki mega-thrust earthquake (M9.0) inverted from strong-motion data, *Geophys. Res. Lett.* **38**, L00G16, doi: [10.1029/2011GL049136](https://doi.org/10.1029/2011GL049136).
- Tajima, F., J. Mori, and B. L. N. Kennett (2013). A review of the 2011 Tohoku-Oki earthquake (M_w 9.0): Large-scale rupture across heterogeneous plate coupling, *Tectonophysics* **586**, 15–34.
- Wei, S., R. Graves, D. Helmberger, J.-P. Avouac, and J. Jiang (2012). Source of shaking and flooding during the Tohoku-Oki earthquake: A mixture of rupture styles, *Earth Planet. Sci. Lett.* **333/334**, 91–100.
- Yagi, Y., and Y. Fukahata (2011). Rupture process of the 2011 Tohoku-Oki earthquake and absolute elastic strain release, *Geophys. Res. Lett.* **38**, L19397, doi: [10.1029/2011GL048701](https://doi.org/10.1029/2011GL048701).
- Yagi, Y., A. Nakao, and A. Kasahara (2012). Smooth and rapid slip near the Japan Trench during the 2011 Tohoku-Oki earthquake revealed by a hybrid back-projection method, *Earth Planet. Sci. Lett.* **355/356**, 94–101.
- Yoshida, Y. (2011). Source process of the 2011 Off the Pacific Coast of Tohoku earthquake with the combination of teleseismic and strong motion data, *Earth Planets Space* **63**, no. 7, 565–569.
- Yue, H., and T. Lay (2011). Inversion of high-rate (1 sps) GPS data for rupture process of the 11 March 2011 Tohoku earthquake (M_w 9.1), *Geophys. Res. Lett.* **38**, no. 7, L00G09, doi: [10.1029/2011GL048700](https://doi.org/10.1029/2011GL048700).
- Zhang, Y., R. Wang, J. Zschau, Y. T. Chen, S. Parolai, and T. Dahm (2014). Automatic imaging of earthquake rupture processes by iterative deconvolution and stacking of high-rate GPS and strong motion seismograms, *J. Geophys. Res.* **119**, no. 7, 5633–5650.

Swiss Seismological Service
ETH Zurich
Sonnegstrasse 5
8092 Zürich
Switzerland
percy.galvez.barron@gmail.com
(P.G.)

swissnuclear
Aarauerstrasse 55
4601 Olten
Switzerland
luis.dalguer@swissnuclear.ch
(L.A.D.)

Seismological Laboratory
California Institute of Technology
1200 E California Boulevard
Pasadena, California 91125
ampuero@gps.caltech.edu
(J.-P.A.)

Institute of Geophysics
ETH Zurich
Sonnegstrasse 5
8092 Zurich
Switzerland
domenico.giardini@erdw.ethz.ch
(D.G.)

Manuscript received 11 March 2016;
Published Online 24 May 2016